Striosome–dendron bouquets highlight a unique striatonigral circuit targeting dopamine-containing neurons

Jill R. Crittenden[a,b,c], Paul W. Tillberg[d,e], Michael H. Riad[a,b], Yasuyuki Shima[f,g], Charles R. Gerfen[h], Jeffrey Curry[a,b], David E. Housman[c], Sacha B. Nelson[f,g], Edward S. Boyden[a,b,d,e,i], and Ann M. Graybiel[a,b,1]

[a]McGovern Institute for Brain Research, Massachusetts Institute of Technology, Cambridge, MA 02139; [b]Department of Brain and Cognitive Sciences, Massachusetts Institute of Technology, Cambridge, MA 02139; [c]Department of Biology, Massachusetts Institute of Technology, Cambridge, MA 02139; [d]Department of Electrical Engineering and Computer Science, Massachusetts Institute of Technology, Cambridge, MA 02139; [e]Massachusetts Institute of Technology Media Laboratory, Massachusetts Institute of Technology, Cambridge, MA 02139; [f]Department of Biology, Brandeis University, Waltham, MA 02453; [g]National Center for Behavioral Genomics, Brandeis University, Waltham, MA 02453; [h]Laboratory of Systems Neuroscience, National Institute of Mental Health, Bethesda, MD 20814; and [i]Department of Biological Engineering, Massachusetts Institute of Technology, Cambridge, MA 02139

Contributed by Ann M. Graybiel, August 12, 2016 (sent for review August 4, 2016; reviewed by Clifton W. Ragsdale and Clifford B. Saper)

The dopamine systems of the brain powerfully influence movement and motivation. We demonstrate that striatonigral fibers originating in striosomes form highly unusual bouquet-like arborizations that target bundles of ventrally extending dopamine-containing dendrites and clusters of their parent nigral cell bodies. Retrograde tracing showed that these clustered cell bodies in turn project to the striatum as part of the classic nigrostriatal pathway. Thus, these striosome–dendron formations, here termed "striosome–dendron bouquets," likely represent subsystems with the nigro–striato–nigral loop that are affected in human disorders including Parkinson's disease. Within the bouquets, expansion microscopy resolved many individual striosomal fibers tightly intertwined with the dopamine-containing dendrites and also with afferents labeled by glutamatergic, GABAergic, and cholinergic markers and markers for astrocytic cells and fibers and connexin 43 puncta. We suggest that the striosome–dendron bouquets form specialized integrative units within the dopamine-containing nigral system. Given evidence that striosomes receive input from cortical regions related to the control of mood and motivation and that they link functionally to reinforcement and decision-making, the striosome–dendron bouquets could be critical to dopamine-related function in health and disease.

dopamine | striosome | striatum | expansion microscopy

The dopamine-containing nigrostriatal pathway is centrally implicated in the modulation of movement, motivation, and reinforcement-based learning, and its progressive degeneration is a hallmark of Parkinson's disease. A reciprocal striatonigral pathway, returning to the dopamine-containing neurons of the substantia nigra pars compacta (SNc), is thought to regulate the activity of the dopamine-containing SNc neurons, potentially affecting nigrostriatal tract function as well as local dopamine release from ventrally extending dendrites of SNc neurons (1). Strikingly, this striatonigral pathway has been shown to originate mainly from the striosomal compartment (also known as "patches") of the striatum (2–4). These findings suggest that the classic nigro–striato–nigral loop directly incorporates the striosomal system of the striatum.

This possibility is of great interest, because striosomes are in a position to modulate and transmit signals to the SNc from limbic regions of the neocortex that are known to be dysregulated in mood disorders in humans (5, 6). Despite much experimental work, however, the fundamental architecture of striosomal fiber arborizations within the substantia nigra (SN) and their relation to the recipient dopamine-containing neurons has remained unknown. We used protein-retention expansion microscopy (ProExM) (7) and confocal imaging to resolve these terminal domains in relation to dopamine transporter (DAT)-labeled dopamine-containing elements of the SNc in three lines of mice engineered to express fluorescent tags preferentially in striosomal neurons (Fig. 1 *A–F* and Fig. S1 *A–C*). We compared these patterns with the patterns found in a line with matrix-predominant fluorophore expression (Fig. 1 *G–I*) (8–11). For convenience, we refer to these mouse lines as the "striosome" and "matrix" lines, but we recognize that none is fully restricted to a single compartment and that selectivity for striosomes is regional.

Results

Striosome-Reporter Mice Display Entwined Striosomal Fibers and Dopamine-Containing Dendrites in the SN. In each striosome line, fluorophore-labeled putative striosomal axons were aligned along and were intertwined with ventrally extending dendrites collected into prominent bundles (here termed "dendrons") emerging from clusters of ventrally situated dopamine-containing cell bodies (Fig. 1 *J–O* and Fig. S1 *D–F*). By contrast, the matrix-enriched mouse line exhibited enriched fluorophor labeling in the surrounding substantia nigra pars reticulata (SNr) (Fig. 1 *P–R*). Together, the striosomal innervation and innervated nigral dendrons had the appearance of a bouquet whose flowers are the clustered dopamine-containing cell bodies and whose stems are made up of tightly entwined fibers and dendrites (Fig. 2 *A* and *B*).

With ProExM tissue expansion and imaging, we resolved the intimate arrangement of the striosomal axons and dopaminergic processes within the dendrons (Fig. 2 *C–F* and Fig. S2). In the striosome lines P172-mCitrine and Sepw1-Cre NP67 with the Ai14 reporter (9), the proportion of striosomal fibers to

Significance

The dopamine-containing nigrostriatal system and its return striatonigral pathway form a loop–circuit crucial for the functions of dopamine in modulating movement and mood. Here we identify a specialized subsystem within this loop. With new mouse models and tissue expansion to allow nanoscale imaging, we demonstrate that striatonigral fibers originating in striosomes form bouquet-like arborizations innervating clusters of dopamine-containing neurons and their ventrally extending, tightly bundled dendrites. Within these formations (termed "striosome–dendron bouquets"), striosomal axons and dopamine-containing dendrites are intimately intertwined, as are other afferent and glial elements. The stunning selectivity of striosomal output to the bouquets suggests that the bouquets could exert powerful and focused control over elements of the dopamine system in normal and abnormal states.

Author contributions: J.R.C. and A.M.G. designed research; J.R.C., P.W.T., M.H.R., J.C., and A.M.G. performed research and imaging; Y.S., C.R.G., D.E.H., S.B.N., and E.S.B. contributed new reagents/analytic tools; J.R.C., P.W.T., M.H.R., and A.M.G. analyzed data; and J.R.C. and A.M.G. wrote the paper.

Reviewers: C.W.R., University of Chicago; and C.B.S., Harvard Medical School, Beth Israel Deaconess Medical Center.

The authors declare no conflict of interest.

[1]To whom correspondence should be addressed. Email: graybiel@mit.edu.

This article contains supporting information online at www.pnas.org/lookup/suppl/doi:10.1073/pnas.1613337113/-/DCSupplemental.

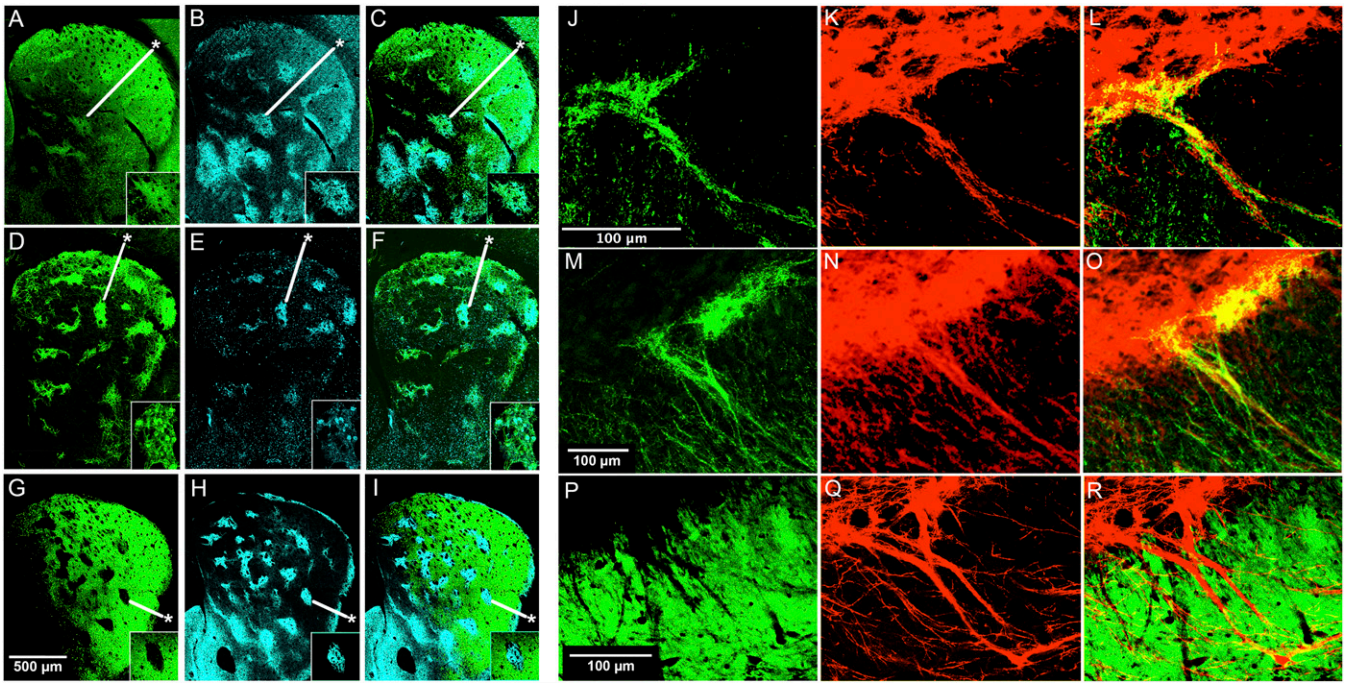

Fig. 1. Projections from striosomes, but not from matrix, target dopamine-containing dendrons in the SN. (*A*, *D*, and *G*) Confocal images of striatum with striosome-predominant fluorophore labeling (*A*; $n = 30$ sections from 5 animals), P172-mCitrine labeling (*D*; $n = 24$ sections from 4 animals), and matrix-predominant labeling (*G*; $n = 30$ sections from 10 animals) in the CalDAG-GEFI-GFP line. (*B*, *E*, and *H*) The same sections with μ-opioid receptor coimmunolabeling of striosomes for all lines ($n = 4$–8 sections from 2 animals). (*C*, *F*, and *I*) Corresponding merged images. (*Insets*) Examples of striosomes (asterisks). (*J*, *M*, and *P*) Fluorophore labeling of dendrons in the SN of CalDAG-GEFII (*J*; $n = 10$ sections from 5 animals) and P172 (*M*; $n = 16$ sections from 4 animals) striosome lines and a near-lack of dendron labeling in the CalDAG-GEFI matrix line (*P*; $n = 6$ sections from 2 animals). (*K*, *N*, and *Q*) the same sections with DAT immunolabeling of dendrons. (*L*, *O*, and *R*) Merged images.

dopamine-containing fibers appeared to be highest in the ventral portions of the dendron (Fig. 2 *C*–*F* and Fig. S1 *D*–*F*). The striosome–dendron bouquets included up to dozens of DAT-positive dendrites and as many striosomal axons.

Markers for GABAergic, Glutamatergic, Cholinergic, and Astrocytic Transmission Are Present Within the Striosome–Dendron Bouquet. We tested for the expression of a series of neurotransmission markers in these striosome–dendron formations. We found immunolabeling for GAD65/67, a presynaptic marker for GABAergic signaling (Fig. 3 *A* and *B*), as well as for VGluT2, a presynaptic marker for glutamatergic signaling (Fig. 3 *C* and *D*). The expression of the D2 receptor (D2R) reporter (Fig. 3 *E* and *F*) and μ-opioid receptor (Fig. 3 *E* and *G*) was high, presumably because of D2 autoreceptor expression in dopamine-containing neurons and μ-opioid receptor expression in striosomal projection neurons. Expression of D1 receptor (D1R) reporters was visible in the neuropil of the SNr and, albeit somewhat more weakly, along and within the dendrons (Fig. 3 *E* and *H* and Fig. S3 *A*–*C*), as tested in D2-GFP;D1-tdTomato double-transgenic and D1-GFP BAC reporter mouse lines (8, 12), indicating that D1-positive striatal projection neurons project to the dendrons but are not enriched there relative to the surrounding SNr. Evidence that the D1-positive inputs to the dendrons were from striosomes was obtained by ProExM in a striosome-mCitrine;D1-tdTomato double-transgenic mouse in which striosome reporter-positive fibers were double-labeled for the D1 reporter (Fig. S3 *D*–*L*). ProExM further allowed resolution of striosome-mCitrine reporter–labeled contacts, potentially synaptic, juxtaposed to DAT-positive dopamine-containing processes (Fig. 3*I*). We detected cholinergic axons and putative terminals within the dendron formations in both ChAT-Cre-Ai32 (13, 14) knock-in mice (Fig. 3*J*, Figs. S4 *A*–*I* and S5, and Movie S1) and ChAT-ChR2-EYFP BAC transgenic mice (15) (Fig. S4 *J*–*L*). Astrocytes and their processes, labeled for GFAP and connexin 43, were displayed at similar densities within the striosome–dendron bouquets and the surrounding SNr (Fig. 3 *K* and *L* and Fig. S6). The relative level of GFAP expression was weaker in the overlying SNc (Fig. S6*A*), as previously reported for astrocytes in the SNc vs. SNr in rats (16), indicating that there may be astrocytic functions that are particular to the ventrally extending dendrite regions of the dopamine-containing neurons.

Striosome–dendron bouquets were evident across the medial–lateral axis of the SN in all striosome lines, despite their different striosome-favoring striatal gradients and different labeling patterns elsewhere. This commonality suggests that striosomal inputs to the dendrons could allow region-selective striatonigral modulation while subserving common higher-order functions because of the similarity in their terminal arborizations. We did not, however, interrogate the entire striosomal system or its internal gradients and bicompartmental patterns (17). We confirmed (3) that, in the posterior SNc, striosomal axons deep in the SNr arborized near clusters of dopamine-containing neurons and ventrally extending processes (Fig. S7); these ventral neurons point to further potential sites of striatonigral input from striosomes.

Nigral Dopamine-Containing Neurons with Dendrons Project to the Dorsal Striatum. Building on prior studies (2–4), with ProExM we were able to resolve both striosome-derived inputs and other afferent fiber systems tightly comingling with the bundled dendrites of the bouquets, suggesting rich synaptic and potentially nonsynaptic interactions within the bouquets and indicating that the bouquets could form relatively discrete integrative units within the dopamine-containing nigral system as a whole. Moreover, we found that these clusters of dopamine-containing cell bodies in the bouquets project to the dorsal striatum, as evidenced by their retrograde labeling in DAT-Cre mice intrastriatally injected with viral vectors carrying a Cre-dependent transgene, as were the dopamine-containing neurons clustered deep within the SNr (Fig. 4 and Fig. S8). In DAT-Cre mice (18), expression of the virally introduced transgene (GCaMP6, detected with an antibody against GFP) was restricted to DAT-positive neurons that project to the site of viral injection (the dorsal striatum).

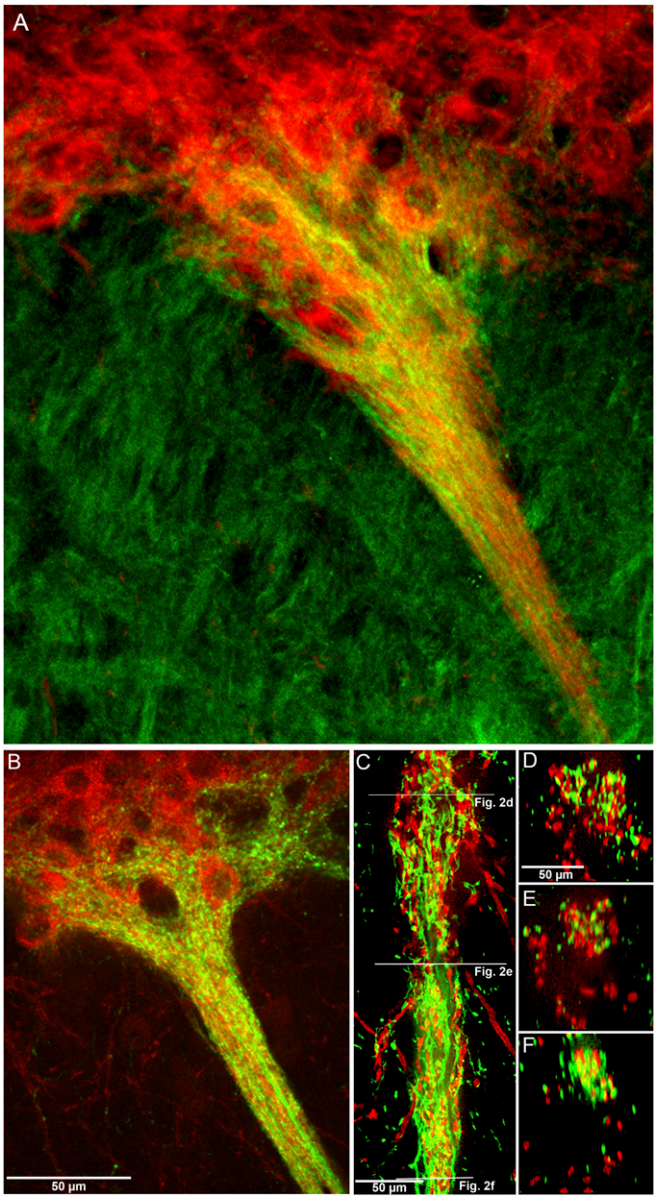

Fig. 2. Striosome–dendron bouquets resolved with confocal microscopy and ProExM. (*A* and *B*) Confocal images of SNc neurons and their ventrally extending dendrites (red) and striosomal axons (green) in the CalDAG-GEFII-GFP (*A*; $n = 9$ sections from 3 animals) and P172-mCitrine (*B*; $n = 12$ sections from 3 animals) striosome lines. Tightly entwined striosomal and dopaminergic fibers in dendrons appear mainly yellow. (*C–F*) ProExM imaging of the bouquet shown in *B* resolves individual striosomal fibers (green) and dendrites (red) in a longitudinal view (*C*) and in cross-sections at three levels (*D–F*) corresponding to the lines drawn in *C*. Similar results were obtained with ProExM in the CalDAG-GEFII-GFP line (Fig. S2). (The scale bar in *B* indicates the dimension of the unexpanded tissue, and the scale bars in *C* and *D* indicate the dimension of the expanded tissue.)

Discussion

The dopamine-containing neurons of the SN receive inputs from multiple sources, as befits their pivotal position in modulating many forms of behavior (19–21). Striatonigral inputs are reported to exert direct inhibition over nigral dopamine-containing neurons (22). The ventrally extending dendrites of these nigral neurons are reported to release dopamine (1), resulting in negative modulation of the dopamine-containing neurons via D2Rs and positive modulation of D1R-bearing terminals that inhibit GABAergic neurons of the nigral complex (23). The ventrally extending dendrites in particular have been suggested to mediate inhibition of dopamine cell firing in response to aversive stimuli (24). If striosomal afferents of the striosome–dendron bouquets affect dopamine release in the SNr, they could regulate the movement-related and motivational functions of the SNr. The tight bundling of GABAergic, glutamatergic, cholinergic, and astrocytic processes within the bouquets further suggests that these inputs could exert combinatorial control over the spike timing of the subclusters of nigral neurons within the bouquets.

The striosomal system and its corticostriatal afferent circuits have been implicated in reinforcement-related functions, including conflict decision-making (6), perhaps by acting as responsibility signals (25) indicating state value (26). Striosomes are reported to be differentially affected in clinical conditions ranging from Huntington's disease and Parkinson's disease to addictive states (27). The unique configuration of striosomal projections to the striosome–dendron bouquets shown here could prove to be a critical determinant of nigro–striato–nigral loop function.

Potential Functional Effects of the Striosome–Dendron Circuit. There is still uncertainty about how distant and local afferents might control local dopamine release by the ventrally extending dendrites of SNc neurons. Given the mounting evidence for GABA release by dopaminergic neurons (28), further effects beyond control of dopamine release could be predicted, either locally or within regions innervated by SNc neurons. Moreover, axons originating from striosomal neurons have collaterals, at least in rodents, that innervate the pallidum (globus pallidus and/or entopeduncular nucleus), again suggesting the potential for widespread effects of the striosomal system (3). This span, as well as the direct targeting of dopamine-containing neurons of the bouquets by striosomal neurons, could account for the strikingly large effects that manipulation of the dorsomedial striosomal system has on many aspects of behavior, from deliberative action selection (29, 30), to drug-induced stereotypy (31, 32), to decision-making under conflict conditions (6). Misgeld and coworkers (23) have suggested that dopamine released locally in the SN can "reinforce D1R mediated activation of striatal projection neurons that inhibit the inhibitory output neurons of the basal ganglia in the substantia nigra." This scenario would potentially cast the striosomes and the striosome–dendron bouquets as regulating release functions of the nigro–striato–nigral system, possibly via control of the dopamine dendrites. If so, this regulation would suggest a particularly interesting but still hypothetical way for mood- and affect-related signals, via striosomes and their projections to the bouquets, to affect responses to external or internal cues.

Cholinergic Input to the Striosome–Dendron Bouquets. A striking finding of this study is that cholinergic fibers, as detected in two different mouse lines engineered to allow their detection, participate in the striosome–dendron bouquets. This evidence builds on prior descriptions of a cholinergic synaptic input to the SNc (33) and extends this evidence by showing that some of these cholinergic fibers target the striosome–dendron bouquets. Much evidence suggests that cholinergic interneurons in the striatum can exert powerful control over the intrastriatal release of dopamine (34, 35). We have noted that these cholinergic interneurons, although having predominant distributions at the striosome–matrix compartment borders (36), send many fine fibers into the striosomes (37, 38). By contrast, cholinergic inputs from the brainstem pedunculopontine nucleus (PPN) preferentially innervate the matrix (39). The PPN innervation of the midbrain (40–42) has been found to regulate locomotor- and aversion-related subcircuits within the SNc and ventral tegmental area, respectively (42, 43), and dopamine-containing nigral neurons express nicotinic and muscarinic acetylcholine receptors (34, 35, 44, 45) and receive synaptic contacts from cholinergic neurons (33). Our findings suggest that the striosome–dendron bouquets also could be important

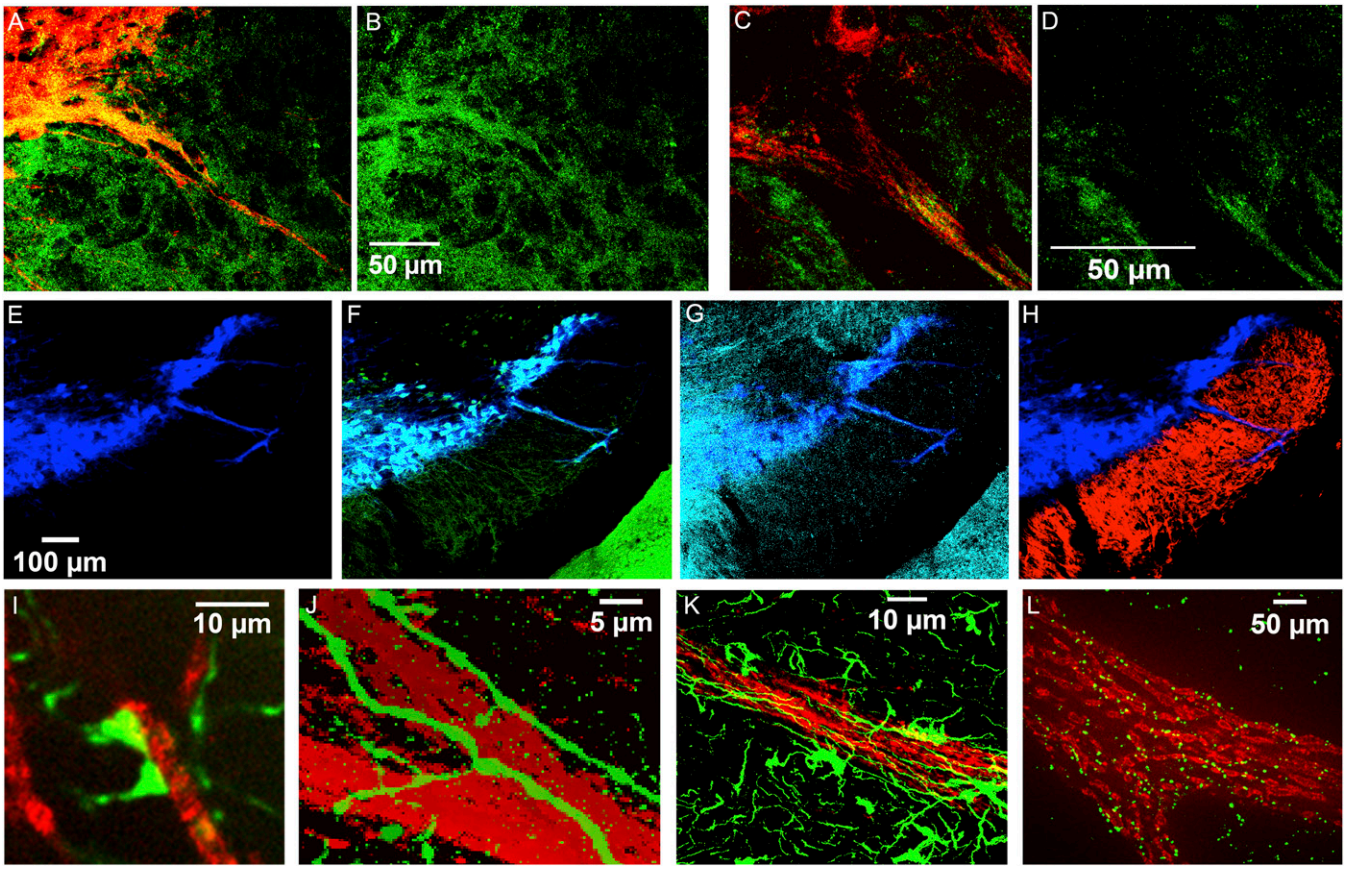

Fig. 3. Immunomarkers identify multiple afferents within striosome–dendron bouquets. (*A–D*) Merged images of DAT-immunolabeled dendrons (red) coimmunolabeled for GAD65/67 (*A* and *B*; $n = 10$ sections from 5 animals) or VGluT2 (*C* and *D*; $n = 10$ sections from 2 animals) (green). (*E–H*) DAT-immunolabeled dendron (blue, *E*) coimmunolabeled for D2-GFP (green, *F*) and μ-opioid receptor (cyan, *G*) and weakly labeled with D1-tdTomato (red, *H*) ($n = 3$ sections from 1 animal). Similar results were obtained with a related line and by ProExM (Fig. S3). The edge of the cerebral peduncle is visible at the lower right corners in *F* and *G* and is immunolabeled for D2-GFP and μ-opioid receptor. (*I*) With ProExM, two mCitrine-positive (green) presumed contacts onto a DAT-positive (red) fiber are visible in the P172 striosome line ($n = 2$ sections from 1 animal). (*J–L*) Single-plane confocal images at the centers of dendrons (immunolabeled for DAT in red) showing cholinergic fibers (green) aligned along and within the dendron in the ChAT-Cre knock-in line with the Ai32-YFP reporter (*J*; $n = 4$ sections from 1 animal; see also Figs. S4 and S5), astrocytes (green, immunolabeled for GFAP) associated with dendron (*K*; $n = 6$ sections from 2 animals; see also Fig. S6 *A–C*), and ProExM of connexin-43 (green) junctions along the dendron (*L*; $n =$ one section from 1 animal; see also Fig. S6 *D–F*, $n = 4$ sections from 1 animal). (Scale bars in *B*, *D*, *E*, *J*, and *K* indicate the dimensions of unexpanded tissue; scale bars in *I* and *L* indicate the dimensions of the expanded tissue.)

contributors to the complex cholinergic–dopaminergic interactions that are characteristic of basal ganglia networks.

Heterogeneity of the Nigral Dopamine System. The dopamine-containing neurons of the SNc appear to be functionally heterogeneous, with spike patterns related to positive or negative reinforcement-related stimuli as well as to particularly salient stimuli (see ref. 46 for a review). Heterogeneity in dopamine-containing single-fiber activity has also been shown (ref. 47 and references therein). Our results open the possibility that the dopamine-containing cell clusters of the bouquets, by virtue of their particularly strong input from striosomes, could form specialized nigral compartments related to particular functional response properties of SNc neurons.

The Nigro–Striato–Nigral Loop. The dopamine-containing cell bodies of the bouquets are in spaced clusters and lie within a tier of densely packed nigral neurons that lies just dorsal to the SNr. To test whether these nigral neurons project to the dorsal striatum, we injected the dorsal striatum of DAT-Cre mice with adeno-associated virus 9 (AVV9) carrying the transgene GCaMP6, which encodes a green-fluorescent molecule that we detected with anti-GFP antibody, driven by the cytomegalovirus enhancer-chicken beta-actin promoter (CAG), and which is expressed only after Cre-mediated flip-excision of the Flex cassette. This transgene construct is termed CAG-Flex-GCaMP6m. With these injections, we identified retrogradely labeled SNc neurons that contribute to the striosome–dendron bouquets, as well as DAT-positive cells dorsal to the cell clusters and deeply situated cells of posterior cell clusters. This set of observations suggests that the groups of dopamine-containing bouquet cells that are targeted by the striosomes represent not only specialized components of the striatonigral circuit but also specialized components of the nigrostriatal circuit. Accordingly, signal integration in the striosome–dendron bouquets might regulate dopamine release in the dorsal striatum directly as well as indirectly.

We were unable in these experiments to determine the degree to which these two circuits formed closed loops. Following the intrastriatal viral tracer injections, we observed a patchy pattern of infected striatal neuropil (presumably dopaminergic) and confirmed this preferential labeling to be in striosomes, including the most lateral striosomal feature that curves along the lateral border of the caudoputamen (the so-called "subcallosal streak"). The streak is known to project to dopamine-containing neurons that lie deep in the posterior SNr (3), possibly corresponding to the posterior cell cluster that we identified as projecting back to the dorsal striatum.

The preferential striosome labeling observed in our DAT-Cre retrograde labeling experiments could reflect preferred viral infection or transgene expression in dopaminergic neurons that innervate the striosomes. Alternatively, the neuropil density from infected neurons might be higher in the striosomes than in the surrounding matrix. It

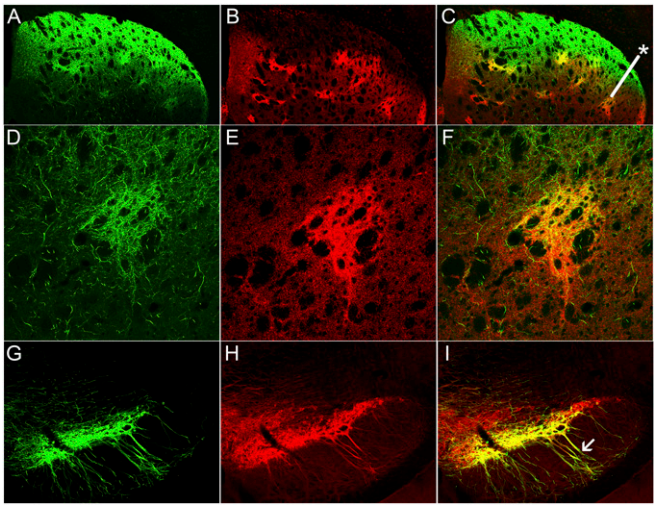

Fig. 4. Subsets of DAT-positive nigral neurons project to the dorsal striatum with a pattern of enriched neuropil labeling in striosomes. (*A* and *B*) Dorsal striatal sections from a DAT-Cre mouse after an intrastriatal injection of AAV9 carrying a CAG-Flex-GCaMP6m expression construct, showing axon terminals that are labeled for GCaMP6 (immunoreactive for anti-GFP, in green) (*A*) in striosomes identified by μ-opioid receptor immunoreactivity (red) (*B*). (*C*) Merged image ($n = 9$ sections from 6 animals). (*D* and *E*) High magnification of a striosome (identified by the asterisk in *C*) with enriched GCaMP6-positive neuropil relative to the surrounding matrix (*D*), as identified by μ-opioid receptor immunoreactivity (*E*). (*F*) Merged image. (*G* and *H*) A nigral section from the mouse shown in *A* showing AAV9-mediated expression of GCaMP6 (*G*) in a ventral layer of the DAT-positive (red) nigral neurons (*H*). (*I*) Merged image ($n = 12$ sections from 6 animals). The arrow in *I* designates a dendron that is double-labeled for GCaMP6 and DAT. See also Fig. S8.

is reported that individual dopamine-containing neurons that lie ventrally or along the SNc/SNr border, which given our findings likely include neurons that form the dendrons of the striosome–dendron bouquets, target both striatal compartments, with a notable preference for striosomes (48–50).

Nigral sections from all mice with intrastriatal injections of AAV9 carrying CAG-Flex-GCaMP6m, whether medially or laterally placed (see *Materials and Methods* for coordinates), exhibited DAT-Cre–mediated GCaMP6 expression in the dopamine-containing dendrons and their parent neurons of the bouquets as well as in dopamine-containing neurons located along the dopamine-containing dendrons and the putative posterior cell cluster. Dopamine release and activity in the striosomes and matrix are differentially regulated, including by psychomotor stimulants (31, 51–53); whether such control is related to input from the dopamine cell clusters and dendrons of the bouquets remains to be investigated.

Potential Relevance to Parkinson's Disease. In a mouse developmental model of Parkinson's disease ($Pitx3^{ak/ak}$ mice), degeneration occurs in a subpopulation of ventrally situated SNc neurons negative for the calcium-binding protein calbindin-D28k (54). Postmortem studies of the human brain have found clusters of neurons (nigrosomes) that are calbindin poor, and in the brains of individuals diagnosed as having Parkinson's disease these nigrosomes are lost in a particular order, apparently according to progressive stages of the disease (55, 56). It will be of great interest to learn how these clustered formations relate to the cell clusters of the striosome–dendron bouquets.

Materials and Methods

Animals. The Committee on Animal Care at the Massachusetts Institute of Technology approved all experimental protocols for work with mice. Male and female mice were given free access to food and water and were maintained on a 12/12-h light/dark cycle (light on at 7:00 AM). All mice were hemizygous or heterozygous. Mice were genotyped for *GFP*, *tdRFP*, *YFP*, and gene-specific BAC constructs by Transnetyx, Inc. P172 mice were used at age 3.5–5.5 wk because of age-dependent silencing of the transgene. The other mice were evaluated at age 8–16 wk, except for three of the six DAT-Cre mice, which were evaluated at age 1.8 y. The genotypes and genetic backgrounds of the mice are listed in Table S1.

Perfusion. Mice were deeply anesthetized with an overdose of Euthasol (Virbac AH Inc.; pentobarbital sodium and phenytoin sodium) and then were perfused with 0.9% saline, followed by 4% (wt/vol) paraformaldehyde in 0.1 M $NaKPO_4$ buffer. Brains then were removed from the calvarium, postfixed for 90 min, stored in 25% (vol/vol) glycerol sinking solution overnight, and cut into transverse 30-μm sections on a freezing microtome. Sections were stored in 0.1% sodium azide in 0.1 M phosphate buffer solution (PBS) made from $NaKPO_4$.

Immunolabeling. Sections were given three successive 2-min rinses in 0.01 M PBS with 0.2% Triton X-100 and then were exposed for 20 min to Tyramide Signal Amplification (TSA) Blocking Reagent (Perkin-Elmer). Immunofluorescence was performed with primary antibodies (Table S2) suspended in TSA Blocking Reagent for 48 h at 4 °C on a shaker. Following primary incubation, sections were rinsed three times for 60 min in 0.01 M PBS with 0.2% Triton X-100 and were incubated in secondary antibodies suspended in TSA Blocking Reagent for 24 h at room temperature. For confocal microscopy, Alexa Fluor secondary antibodies (Thermo Fisher Scientific) were used (Table S3). Following secondary incubation, sections were rinsed three times for 60 min in 0.1 M PBS. For confocal microscopy, sections were mounted on subbed glass slides and were coverslipped using ProLong Antifade Reagent (Thermo Fisher Scientific). Whole-section montages of high-magnification images were collected using a Zeiss LSM 510 Confocal Microscope with ZEN imaging software. Images were processed and analyzed with Fiji software (57).

For immunohistochemistry to detect retrograde infection with AAV9 harboring a CAG-Flex-GCaMP6m construct, tissue sections were prepared as described above. Sections were incubated with primary antibody against GFP, followed by a biotinylated goat anti-rabbit secondary antibody (Tables S2 and S3). Immunoreactivity was amplified and detected by the Vectastain Peroxidase ABC System (Vector Laboratories). Sections were mounted and coverslipped with Eukitt (Electron Microscopy Sciences). Images were acquired on a Leica stereomicroscope.

ProExM. Antibody-labeled tissue slices were incubated in anchoring solution overnight at room temperature. Acryloyl-X, SE [6-((acryloyl)amino)hexanoic acid, succinimidyl ester, Thermo-Fisher Scientific A20770, here abbreviated "AcX"] was resuspended in anhydrous DMSO at a concentration of 10 mg/mL, aliquoted, and stored frozen in a desiccated environment. AcX prepared this way can be stored for up to 2 mo. Aliquots were thawed and diluted to 0.1 mg/mL AcX in 0.01 M PBS to produce anchoring solution for each use.

AcX-treated sections were gelled, digested, and expanded as described previously (7). Monomer solution [0.01 M PBS, 2 M NaCl, 8.625% (wt/wt) sodium acrylate, 2.5% (wt/wt) acrylamide, 0.15% (wt/wt) N,N′-methylenebisacrylamide] was mixed, frozen in aliquots, and thawed before use. Monomer solution was cooled to 4 °C before use. The radical inhibitor 4-hydroxy-2,2,6,6-tetramethylpiperidin-1-oxyl (4-hydroxy-TEMPO) was added up to 0.01% (wt/wt) from a 0.5% (wt/wt) aqueous stock to inhibit gelation during diffusion of the monomer solution into tissue sections. Concentrated aqueous stocks (10% wt/wt) of tetramethylethylenediamine (TEMED) accelerator and ammonium persulfate (APS) radical initiator were added to the monomer solution up to 0.2% (wt/wt) each. Tissue sections were incubated with the monomer solution plus 4-hydroxy-TEMPO/TEMED/APS at 4 °C for 25 min and then were transferred to gelation chambers and, within 30 min after the addition of APS to the monomer solution, were placed in a humidified 37 °C incubator for 2 h for gelation.

Proteinase K (New England Biolabs) was diluted 1:100 (eight units/mL) in digestion buffer [50 mM Tris (pH 8), 1 mM EDTA, 0.5% Triton X-100, 1 M NaCl]. Gels were fully immersed in this solution and then were incubated overnight at room temperature. Digested gels were next placed in excess volumes of doubly deionized water for 15 min to expand. This step was repeated three to five times in fresh water until the size of the expanding sample plateaued.

Postexpansion confocal imaging of cells and fibers was performed on an Andor spinning disk (CSU-X1 Yokogawa) confocal system with a 40× 1.15 NA water objective. To quantify the expansion factor, specimens were imaged pre- and postexpansion on a Nikon Ti-E epifluorescence microscope with a 4× 0.13 NA air objective. Glass-bottomed six-well plates were treated with 0.1 mg/mL poly-L-lysine for 5 min, washed in double deionized water for 5 min, and then dried to adhere gels for stable imaging. Gels were placed in treated wells, left for 5 min, and then were covered in water for imaging. Image stitching was done using the Grid/Collection stitching plugin in ImageJ (58).

Stereotaxic Surgery and Virus Injections. Mice were anesthetized by injection of ketamine (120 mg/kg) and xylazine (16 mg/kg) in saline, and intrastriatal

injections of virus (AAV9-CAG-Flex-GCaMP6m-WPRE.SV40 from The University of Pennsylvania vector core facility) were made with a NanoFil microsyringe (World Precision Instruments). Images shown are from the side of the 0.2-μL virus injections, but we note that retrograde labeling of dopamine-containing dendrons and posteroventral nigral cells was also observed on the contralateral side in which 0.1 μL of virus was injected. Bilateral injections were made in six mice at the following sites: anteroposterior (AP): +0.9, mediolateral (ML): ±1.8, dorsoventral (DV): −2.0 (DAT-Cre mouse no. 152 is shown in Fig. S8 *A–F*); AP: +0.9, ML: ±1.9, DV: −2.0 (DAT-Cre mouse no. 154 is shown in Fig. S8 *G–L*); AP: +0.9, ML: ±2.0, DV: −2.0 (DAT-Cre mouse no. 156 is shown in Fig. 4 and Fig. S8 *M–R*). Three weeks after virus injection, mice were transcardially perfused for immunohistology.

ACKNOWLEDGMENTS. We thank Dr. Mark Harnett for helpful discussions; Dr. Yasuo Kubota for text management; and Dr. Dan Hu and Anne C. Kim for technical assistance. This work was supported by William N. and Bernice E. Bumpus Foundation Grant Rapid Response Discovery Award Pilot: 2013.1 (to A.M.G.), the Saks Kavanaugh Foundation (A.M.G.), CHDI Foundation Grant A-5552 (to A.M.G.), the Collaborative Center for X-linked Dystonia Parkinsonism at Massachusetts General Hospital (J.R.C. and A.M.G.), the McGovern Institute for Brain Research (A.M.G. and E.S.B.), MIT Media Laboratory (E.S.B.), and the Open Philanthropy Project (E.S.B.). E.S.B. is the recipient of a New York Stem Cell Foundation-Robertson Investigator Award, and P.T. is the recipient of a Hertz fellowship.

1. Rice ME, Patel JC (2015) Somatodendritic dopamine release: Recent mechanistic insights. *Philos Trans R Soc Lond B Biol Sci* 370(1672):1–14.
2. Gerfen CR (1985) The neostriatal mosaic. I. Compartmental organization of projections from the striatum to the substantia nigra in the rat. *J Comp Neurol* 236(4):454–476.
3. Fujiyama F, et al. (2011) Exclusive and common targets of neostriatofugal projections of rat striosome neurons: A single neuron-tracing study using a viral vector. *Eur J Neurosci* 33(4):668–677.
4. Watabe-Uchida M, Zhu L, Ogawa SK, Vamanrao A, Uchida N (2012) Whole-brain mapping of direct inputs to midbrain dopamine neurons. *Neuron* 74(5):858–873.
5. Eblen F, Graybiel AM (1995) Highly restricted origin of prefrontal cortical inputs to striosomes in the macaque monkey. *J Neurosci* 15(9):5999–6013.
6. Friedman A, et al. (2015) A corticostriatal path targeting striosomes controls decision-making under conflict. *Cell* 161(6):1320–1333.
7. Tillberg PW, et al. (2016) Protein-retention expansion microscopy of cells and tissues labeled using standard fluorescent proteins and antibodies. *Nat Biotechnol* 34(9):987–992.
8. Gong S, et al. (2003) A gene expression atlas of the central nervous system based on bacterial artificial chromosomes. *Nature* 425(6961):917–925.
9. Madisen L, et al. (2010) A robust and high-throughput Cre reporting and characterization system for the whole mouse brain. *Nat Neurosci* 13(1):133–140.
10. Gerfen CR, Paletzki R, Heintz N (2013) GENSAT BAC cre-recombinase driver lines to study the functional organization of cerebral cortical and basal ganglia circuits. *Neuron* 80(6):1368–1383.
11. Shima Y, et al. (2016) A mammalian enhancer trap resource for discovering and manipulating neuronal cell types. *eLife* 5:e13503.
12. Ade KK, Wan Y, Chen M, Gloss B, Calakos N (2011) An improved BAC transgenic fluorescent reporter line for sensitive and specific identification of striatonigral medium spiny neurons. *Front Syst Neurosci* 5:32.
13. Rossi J, et al. (2011) Melanocortin-4 receptors expressed by cholinergic neurons regulate energy balance and glucose homeostasis. *Cell Metab* 13(2):195–204.
14. Madisen L, et al. (2012) A toolbox of Cre-dependent optogenetic transgenic mice for light-induced activation and silencing. *Nat Neurosci* 15(5):793–802.
15. Zhao S, et al. (2011) Cell type–specific channelrhodopsin-2 transgenic mice for optogenetic dissection of neural circuitry function. *Nat Methods* 8(9):745–752.
16. Kil AC, Crukarch B, Jonker AJ, Groenewegen HJ, Voorn P (2009) Upregulation of NAD (P)H:quinone oxidoreductase (NQO1) in glial cells of 6-hydroxydopamine-lesioned substantia nigra in the rat. *The Basal Ganglia IX,* Advances in Behavioral Biology, eds Groenewegen HJ, Voorn P, Berendse HW, Mulder AB, Cools AR (Springer, New York), Vol 58, pp 411–429.
17. Ragsdale CW, Jr, Graybiel AM (1990) A simple ordering of neocortical areas established by the compartmental organization of their striatal projections. *Proc Natl Acad Sci USA* 87(16):6196–6199.
18. Bäckman CM, et al. (2006) Characterization of a mouse strain expressing Cre recombinase from the 3′ untranslated region of the dopamine transporter locus. *Genesis* 44(8):383–390.
19. Hikosaka O, Bromberg-Martin E, Hong S, Matsumoto M (2008) New insights on the subcortical representation of reward. *Curr Opin Neurobiol* 18(2):203–208.
20. Lerner TN, et al. (2015) Intact-brain analyses reveal distinct information carried by SNc dopamine subcircuits. *Cell* 162(3):635–647.
21. Menegas W, et al. (2015) Dopamine neurons projecting to the posterior striatum form an anatomically distinct subclass. *eLife* 4:e10032.
22. Brazhnik E, Shah F, Tepper JM (2008) GABAergic afferents activate both GABAA and GABAB receptors in mouse substantia nigra dopaminergic neurons in vivo. *J Neurosci* 28(41):10386–10398.
23. Radnikow G, Misgeld U (1998) Dopamine D1 receptors facilitate GABAA synaptic currents in the rat substantia nigra pars reticulata. *J Neurosci* 18(6):2009–2016.
24. Henny P, et al. (2012) Structural correlates of heterogeneous in vivo activity of midbrain dopaminergic neurons. *Nat Neurosci* 15(4):613–619.
25. Amemori K, Gibb LG, Graybiel AM (2011) Shifting responsibly: The importance of striatal modularity to reinforcement learning in uncertain environments. *Front Hum Neurosci* 5:47.
26. Doya K (2000) Complementary roles of basal ganglia and cerebellum in learning and motor control. *Curr Opin Neurobiol* 10(6):732–739.
27. Crittenden JR, Graybiel AM (2016) Disease-associated changes in the striosome and matrix compartments of the dorsal striatum. *Handbook of Basal Ganglia Structure and Function*, eds Steiner H, Tseng K (Elsevier, Amsterdam), 2nd Ed .
28. Tritsch NX, Ding JB, Sabatini BL (2012) Dopaminergic neurons inhibit striatal output through non-canonical release of GABA. *Nature* 490(7419):262–266.
29. Yin HH, Knowlton BJ, Balleine BW (2005) Blockade of NMDA receptors in the dorsomedial striatum prevents action-outcome learning in instrumental conditioning. *Eur J Neurosci* 22(2):505–512.
30. Ito M, Doya K (2015) Distinct neural representation in the dorsolateral, dorsomedial, and ventral parts of the striatum during fixed- and free-choice tasks. *J Neurosci* 35(8):3499–3514.
31. Canales JJ, Graybiel AM (2000) A measure of striatal function predicts motor stereotypy. *Nat Neurosci* 3(4):377–383.
32. Murray RC, Gilbert YE, Logan AS, Hebbard JC, Horner KA (2014) Striatal patch compartment lesions alter methamphetamine-induced behavior and immediate early gene expression in the striatum, substantia nigra and frontal cortex. *Brain Struct Funct* 219(4):1213–1229.
33. Bolam JP, Francis CM, Henderson Z (1991) Cholinergic input to dopaminergic neurons in the substantia nigra: A double immunocytochemical study. *Neuroscience* 41(2-3):483–494.
34. Zhou FM, Liang Y, Dani JA (2001) Endogenous nicotinic cholinergic activity regulates dopamine release in the striatum. *Nat Neurosci* 4(12):1224–1229.
35. Threlfell S, et al. (2012) Striatal dopamine release is triggered by synchronized activity in cholinergic interneurons. *Neuron* 75(1):58–64.
36. Bernácer J, Prensa L, Giménez-Amaya JM (2007) Cholinergic interneurons are differentially distributed in the human striatum. *PLoS One* 2(11):e1174.
37. Graybiel AM, Baughman RW, Eckenstein F (1986) Cholinergic neuropil of the striatum observes striosomal boundaries. *Nature* 323(6089):625–627.
38. Crittenden JR, Lacey CJ, Lee T, Bowden HA, Graybiel AM (2014) Severe drug-induced repetitive behaviors and striatal overexpression of VAChT in ChAT-ChR2-EYFP BAC transgenic mice. *Front Neural Circuits* 8:57.
39. Dautan D, et al. (2014) A major external source of cholinergic innervation of the striatum and nucleus accumbens originates in the brainstem. *J Neurosci* 34(13):4509–4518.
40. Graybiel AM (1977) Direct and indirect preoculomotor pathways of the brainstem: An autoradiographic study of the pontine reticular formation in the cat. *J Comp Neurol* 175(1):37–78.
41. Mena-Segovia J, Winn P, Bolam JP (2008) Cholinergic modulation of midbrain dopaminergic systems. *Brain Res Brain Res Rev* 58(2):265–271.
42. Xiao C, et al. (2016) Cholinergic mesopontine signals govern locomotion and reward through dissociable midbrain pathways. *Neuron* 90(2):333–347.
43. Dautan D, et al. (2016) Segregated cholinergic transmission modulates dopamine neurons integrated in distinct functional circuits. *Nat Neurosci* 19(8):1025–1033.
44. Miwa JM, Freedman R, Lester HA (2011) Neural systems governed by nicotinic acetylcholine receptors: Emerging hypotheses. *Neuron* 70(1):20–33.
45. Inden M, et al. (2016) α4 nicotinic acetylcholine receptor modulated by galantamine on nigrostriatal terminals regulates dopamine receptor-mediated rotational behavior. *Neurochem Int* 94:74–81.
46. Bromberg-Martin ES, Matsumoto M, Hikosaka O (2010) Dopamine in motivational control: Rewarding, aversive, and alerting. *Neuron* 68(5):815–834.
47. Howe MW, Dombeck DA (2016) Rapid signalling in distinct dopaminergic axons during locomotion and reward. *Nature* 535(7613):505–510.
48. Gerfen CR, Herkenham M, Thibault J (1987) The neostriatal mosaic: II. Patch- and matrix-directed mesostriatal dopaminergic and non-dopaminergic systems. *J Neurosci* 7(12):3915–3934.
49. Jimenez-Castellanos J, Graybiel AM (1987) Subdivisions of the dopamine-containing A8-A9-A10 complex identified by their differential mesostriatal innervation of striosomes and extrastriosomal matrix. *Neuroscience* 23(1):223–242.
50. Matsuda W, et al. (2009) Single nigrostriatal dopaminergic neurons form widely spread and highly dense axonal arborizations in the neostriatum. *J Neurosci* 29(2):444–453.
51. Granado N, et al. (2010) Selective vulnerability in striosomes and in the nigrostriatal dopaminergic pathway after methamphetamine administration : Early loss of TH in striosomes after methamphetamine. *Neurotox Res* 18(1):48–58.
52. Brimblecombe KR, Cragg SJ (2015) Substance P weights striatal dopamine transmission differently within the striosome-matrix axis. *J Neurosci* 35(24):9017–9023.
53. Salinas AG, Davis MI, Lovinger DM, Mateo Y (2016) Dopamine dynamics and cocaine sensitivity differ between striosome and matrix compartments of the striatum. *Neuropharmacology* 108:275–283.
54. Luk KC, et al. (2013) The transcription factor Pitx3 is expressed selectively in midbrain dopaminergic neurons susceptible to neurodegenerative stress. *J Neurochem* 125(6):932–943.
55. Damier P, Hirsch EC, Agid Y, Graybiel AM (1999) The substantia nigra of the human brain. II. Patterns of loss of dopamine-containing neurons in Parkinson's disease. *Brain* 122(Pt 8):1437–1448.
56. Schwarz ST, et al. (2014) The 'swallow tail' appearance of the healthy nigrosome - a new accurate test of Parkinson's disease: A case-control and retrospective cross-sectional MRI study at 3T. *PLoS One* 9(4):e93814.
57. Schindelin J, et al. (2012) Fiji: An open-source platform for biological-image analysis. *Nat Methods* 9(7):676–682.
58. Preibisch S, Saalfeld S, Tomancak P (2009) Globally optimal stitching of tiled 3D microscopic image acquisitions. *Bioinformatics* 25(11):1463–1465.

Supporting Information

Crittenden et al. 10.1073/pnas.1613337113

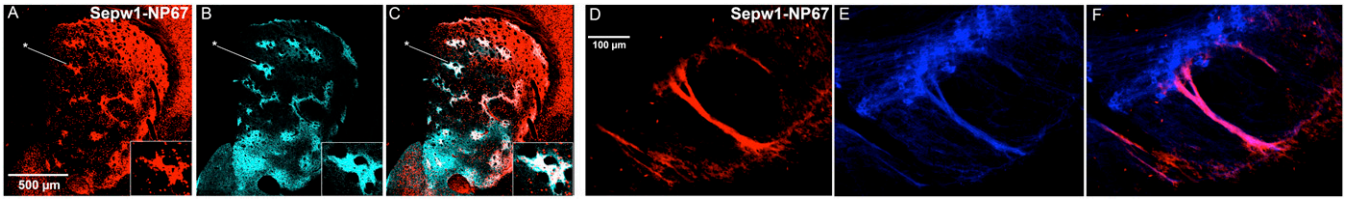

Fig. S1. Striosomes and striosome-dendron bouquets in the striosome line Sepw1-Cre NP67 carrying the Cre-dependent Ai14-tdTomato reporter. (*A* and *B*) Transverse hemisection through the left striatum showing striosomes coimmunolabeled for tdTomato (red) (*A*) and μ-opioid receptor (cyan) (*B*). (*C*) Merged image ($n = 6$ six sections from 2 animals). The reporter expression follows a gradient with compartment-selective expression in the ventromedial striatum that changes to partial filling-in of both compartments in the most dorsal and dorsolateral striatum. Enhanced compartmental selectivity is greater in the medial striatum than in the lateral striatum. *Insets* in *A*–*C* show a striosome (asterisk) at a higher magnification. (*D* and *E*) Transverse hemisections through the left SN showing striosome-dendron bouquets immunolabeled for the striosome Sepw1-Cre NP67 line with Ai14 reporter (red; *D*) and the dopamine transporter (blue; *E*); $n = 6$ sections from 2 animals. (*F*) Merged image. The striosomal fibers run along bundles of descending dendrites that emerge from small clusters of DAT-positive cells situated near the border of the SNc and SNr. The dendrons are distributed along the medial–lateral axis, in this example with regular interspaces. We observed similar patterns of dendrons in mice and rats in which sections through the SN were labeled for tyrosine hydroxylase.

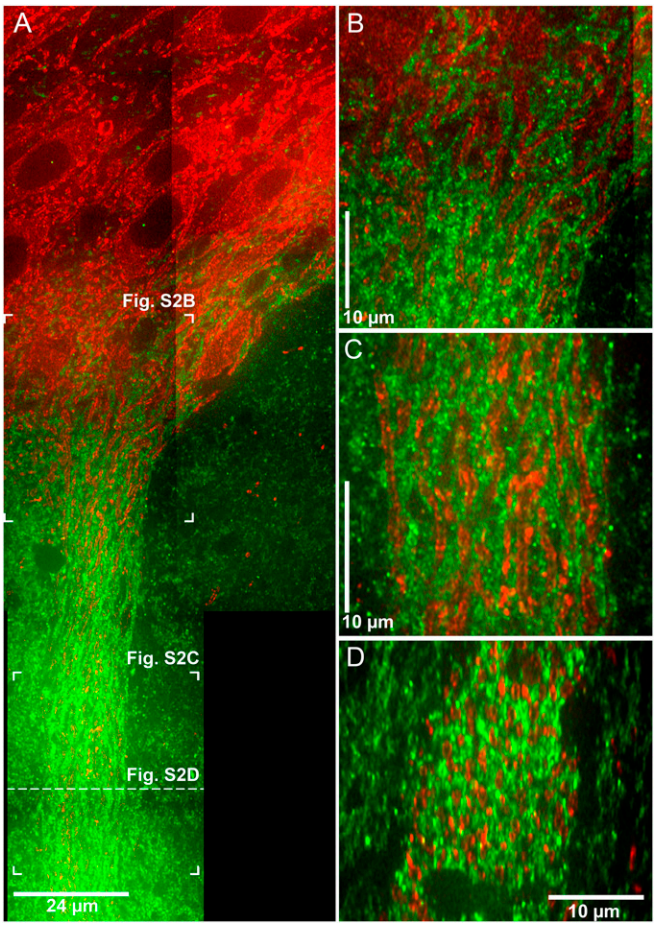

Fig. S2. ProExM view of a striosome-dendron bouquet in the CalDAG-GEFII-GFP BAC striosome line. (*A*) DAT immunolabeling (red) of a cluster of nigral cell bodies with their ventrally extending dendrites interwoven with GFP-labeled putative striosomal fibers ($n = 2$ sections from 2 animals). (*B*) Magnified view at a dorsal level of the bouquet, as indicated by brackets in *A*. The GFP-positive putative striosomal fibers (green) appear to extend dorsally to contact ventrally located DAT-positive nigral cells. (*C*) Magnified view of a more ventral region along the dendron, as indicated in *A*. The DAT-positive dendrites (red) are entwined with many thin GFP-positive fibers. For comparison, see the P172 striosome line image in Fig. 2*C*. (*D*) A cross-section of the dendron made by rotating a Z-stack series of images through the dendron at the level indicated in *A*. See also Fig. 2 *D*–*F*. In this thick dendron, there appear to be more than a dozen DAT-positive fibers and GFP-positive fibers. (Scale bars indicate the dimensions of expanded tissue.)

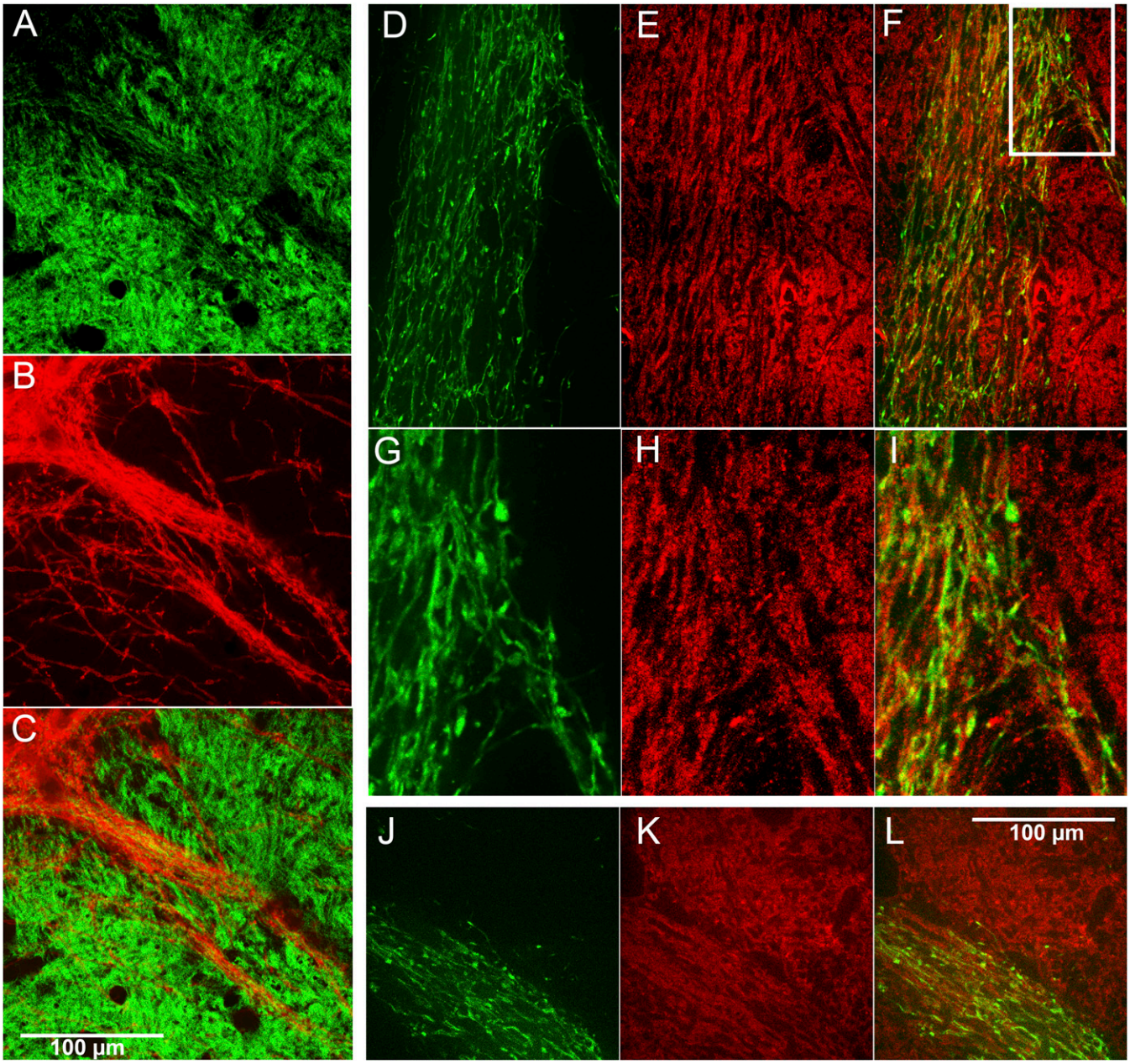

Fig. S3. Expression of the D1 dopamine receptor BAC reporter in the SNr and striosomal fibers of the dopamine-containing dendron. (*A* and *B*) Transverse hemisection through left SN of a D1-GFP BAC reporter line showing moderate GFP immunolabeling of fibers along the dopamine-containing dendron (*A*) colabeled for DAT in red (*B*). (*C*) Merged image. D1-GFP labeling is strong in fibers running in cross-directions in the surrounding SNr ($n = 4$ sections from 2 animals.) (*D–I*) Similar patterns were apparent by ProExM of a dendron and surrounding SNr in a P172-mCitrine;D1-tdTomato double-transgenic line in which the mCitrine immunofluorescence (green) is restricted to the dendron (*D* and *G*), whereas coimmunofluorescence for D1-tdTomato (red) is as bright or brighter in the surrounding SNr (*E* and *H*). Merged images show that the striosome P172-mCitrine–positive fibers are colabeled for D1-tdTomato in this single-plane image from a Z-stack (*F* and *I*). The box in *F* corresponds to the region that is magnified in *G–I*. (*J* and *K*) Direct native fluorescence imaging of the striosome-mCitrine (*J*) and D1-tdTomato (*K*) fluorophores shows the same pattern of colabeling. (*L*) Merged image. (The scale bar in *C* indicates the dimensions of nonexpanded tissue; the scale bar in *L* indicates the dimensions of expanded tissue.)

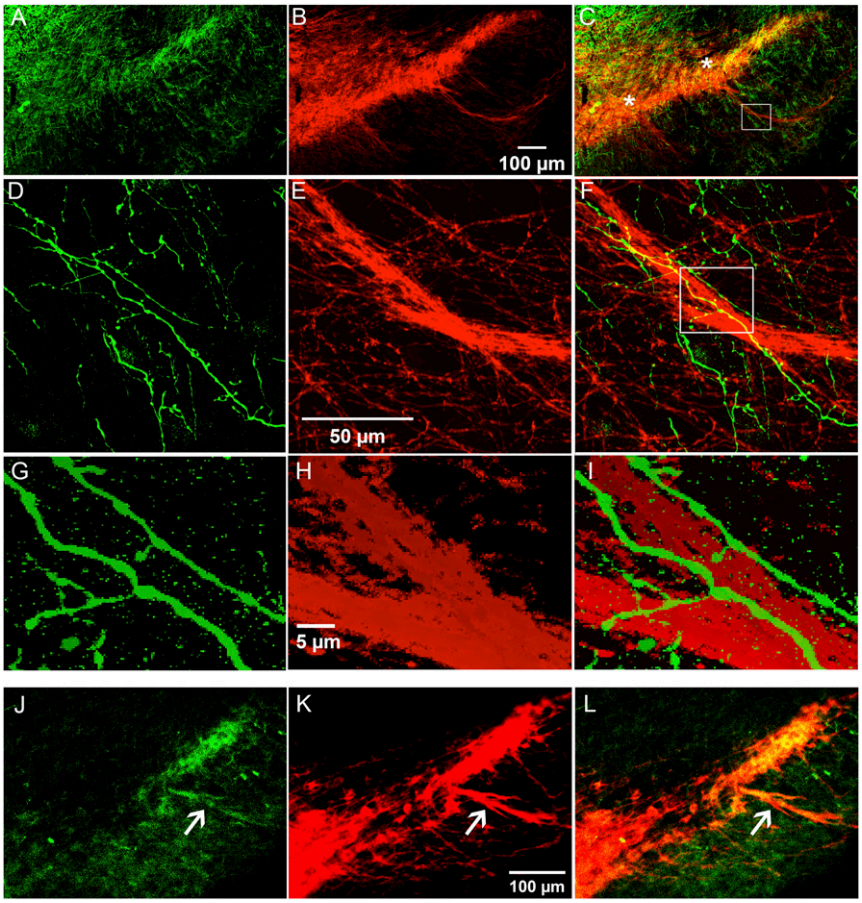

Fig. S4. Sections from the SN of two different cholinergic-reporter mouse lines illustrating cholinergic axons coursing through the SNc and SNr, including within the dopamine-containing dendrons and near their parent dopamine-containing SNc cell clusters. Compare with Fig. 3*J*. (*A*, *D*, and *G*) Successively zoomed-in images of a transverse section through the left SN showing labeling for YFP in the ChAT-Cre knock-in line carrying the Cre-dependent Ai32 YFP reporter. (*B*, *E*, and *H*) The same section coimmunolabeled for DAT (red), with two typical dopamine-containing dendrons and parent cell clusters (indicated by asterisks in *C*). (*C*, *F*, and *I*) Merged images. White boxes in *C* and *F* indicate the successively magnified regions. (*G*, *H*, and *I*) A single Z-plane image through the center of one dendron, illustrating cholinergic fibers branching within the dendron and having bouton-like structures. (*J* and *K*) A section through the SN in a ChATChR2-YFP BAC mouse showing enrichment for the cholinergic YFP reporter in a dopamine dendron (indicated by arrows in *J*, *K*, and *L*) (*J*) and in DAT-positive cells (red) that are located near the border between the SNc and SNr (*K*). (*L*) Merged image; $n = 4$ sections from 1 animal.

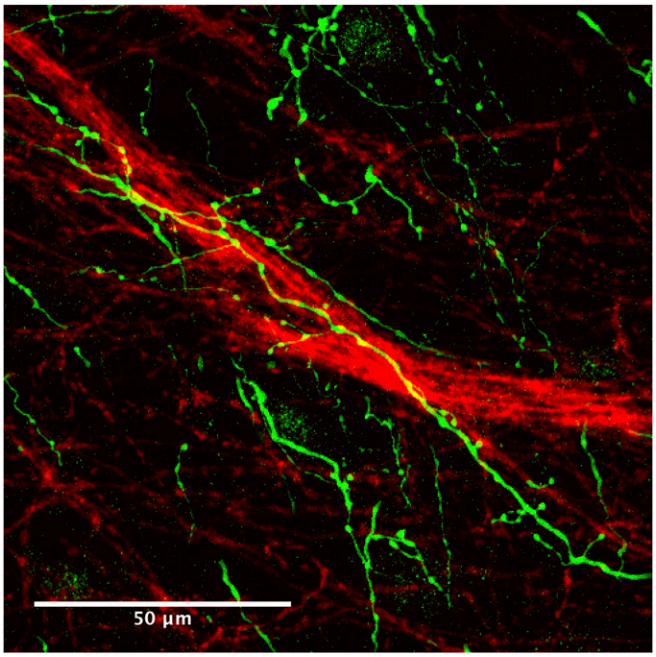

Fig. S5. Maximum projection of a z-series of confocal images, 19.5 µm thick, corresponding to the single-plane image in Fig. 3*J* and Fig. S4*I*, showing cholinergic fibers (green) entwined with the dopamine dendrons (red).

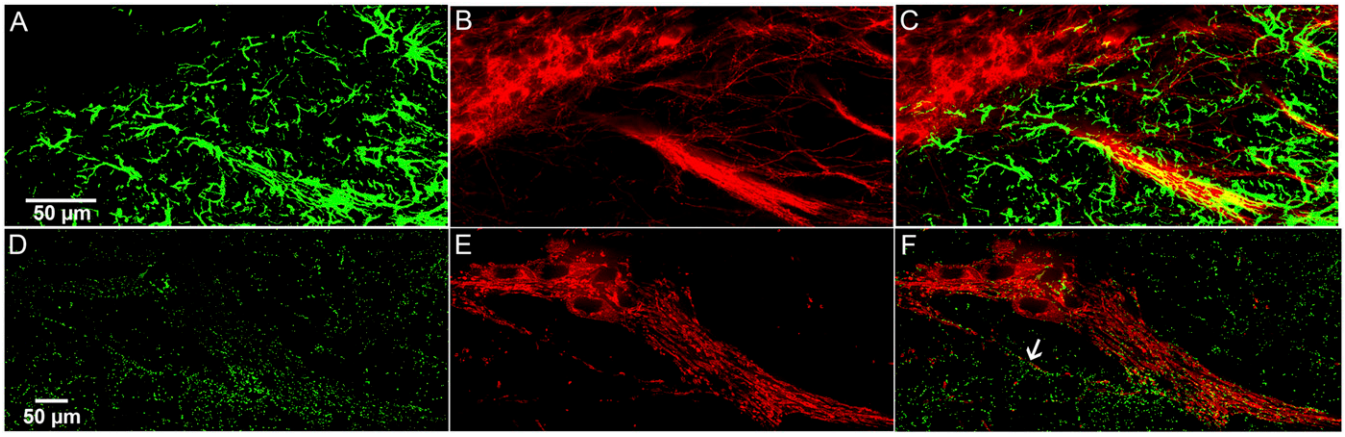

Fig. S6. Astrocytes and the gap junction protein connexin 43 are dispersed along and within the dopamine-containing dendrons as well as in the surrounding SNr. (*A* and *B*) A standard confocal optical section through the center of a dopamine-containing dendron showing astrocytes and their processes labeled for GFAP (green) (*A*) both within and surrounding a DAT-positive dendron (red) (*B*). (*C*) Merged image; $n = 4$ sections from 2 animals. (*D* and *E*) ProExM image of a nigral section coimmunolabeled for connexin 43 (green) (*D*) and DAT (red) (*E*). (*F*) Merged image. Connexin 43-positive puncta are visible alongside single DAT-positive dendrites (arrow in *F*) or dendrites within a dendron (also see Fig. 3*L*). $n = 1$ section from 1 animal. Similar results were obtained with nonexpanded tissues; $n = 4$ sections from 1 animal.

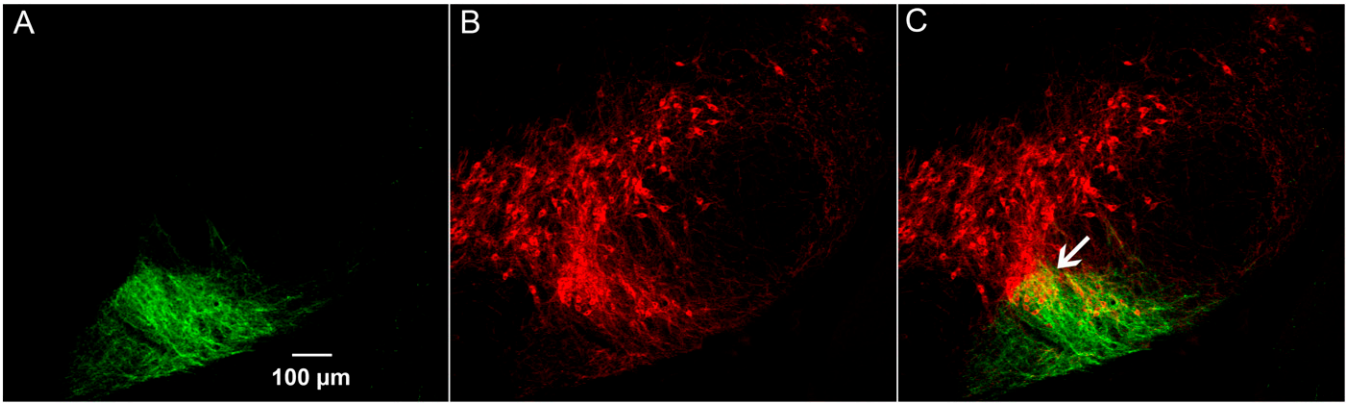

Fig. S7. Striosome-reporter mice have reporter-labeled processes near dopamine-containing cell clusters situated deep in the caudal part of the SN. (*A*) Transverse hemisection through the caudal SN of a P172-mCitrine striosome reporter mouse illustrating labeling in the ventral region; $n = 6$ sections from 2 animals. (*B*) DAT immunolabeling (red) shows that the region targeted by the striosome reporter contains dopamine-containing neurons in a relatively dense cluster, indicated by an arrow in *C*. (*C*) Merged image. This cluster of dopamine-containing neurons possibly corresponds to that previously referred to as the "posterior cell cluster" (3).

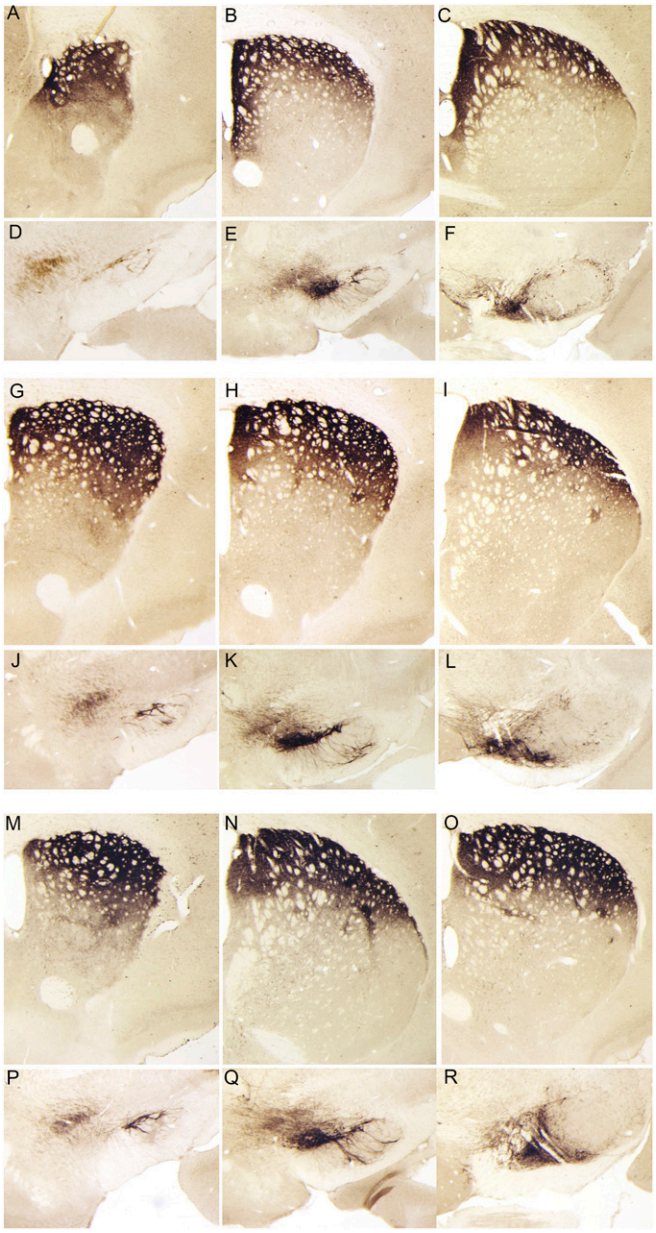

Fig. S8. The dopamine-containing neurons of the striosome–dendron bouquets and of the posterior cell cluster project to the dorsal striatum. (*A–C*, *G–I*, and *M–O*) Transverse hemisection through the left striatum of three DAT-Cre mice that received intrastriatal injections of AAV9 carrying CAG-Flex-GCaMP6m. Anti-GCaMP6 immunoreactivity with anti-GFP antibody (shown in brown) shows dopamine-containing axons in the striatum, which originated from DAT-Cre-positive neurons that were retrogradely infected by AAV9. (*D–F*, *J–L*, and *P–R*) Cell bodies and dopamine-containing dendrons of retrogradely infected DAT-Cre-positive neurons are visible in transverse hemisections through the SN of the mice (*D*, *E*, *J*, *K*, *P*, and *Q*), as well as a posterior cell cluster (*F*, *L*, and *R*); $n = 20$ sections from 6 animals. The GCaMP6 expression is Cre-dependent and therefore is restricted to DAT-Cre–positive nigral neurons that project to the site of viral injection in the dorsal striatum. The intrastriatal viral injections targeted different districts; see *Materials and Methods* for injection coordinates.

Table S1. Transgenic mouse lines

Mouse line and description (ref.)	Genotype	Genetic background
Ai14 knock-in (9) Cre-dependent tdTomato under CAG promoter, inserted at ROSA26 locus	Ai14(RCL-tdT)-D	Mixed C57B6J and 129S1
Ai32 knock-in (14) Cre-dependent channelrhodopsin-YFP fusion protein under CAG promoter, inserted at ROSA26 locus	Ai32(RCL-ChR2(H134R)/EYFP)	Mixed C57B6J and 129S1
CalDAG-GEFI-GFP BAC (8) GFP in CalDAG-GEFI BAC is enriched in D1- and D2-dopamine receptor–positive striatal neurons in the matrix with the most specificity in the medial striatum	Tg(Rasgrp1-EGFP)KX214Gsat/Mmcd	Mixed FVB/N and Swiss Webster
CalDAG-GEFII-GFP BAC (8) GFP in CalDAG-GEFII BAC is enriched in a subset of striosome projection neurons in the medial striatum	Tg(Rasgrp2-EGFP)DU111Gsat/Mmcd	Mixed FVB/N and Swiss Webster
ChAT-IRES-Cre knock-in (13) Cre is downstream of the endogenous ChAT gene with an intervening IRES element and is expressed in cholinergic neurons	B6;129S6-*Chat*$^{tm2(cre)Lowl}$/J	Mixed C57B6/J and 129S6
ChATChR2-YFP BAC (15) Channelrhodopsin-YFP fusion protein in ChAT BAC is overexpressed in cholinergic neurons	B6.Cg-Tg(Chat-COP4*H134R/EYFP,Slc18a3)6Gfng/J	Mixed C57B6/J, FVB/N and 129S6
DAT-IRES-Cre knock-in (18) Cre is downstream of the endogenous DAT gene with an intervening IRES element and is expressed in dopaminergic neurons	Slc6a3tm1.1(cre)Bkmn	C57B6/J
D1-tdTomato BAC (12) tdTomato in Drd1 BAC is expressed in D1-positive striatal neurons	B6.Cg-Tg(Drd1a-tdTomato)6Calak/J	C57B6/J
D1-GFP BAC (8) GFP in Drd1 BAC is expressed in D1-positive striatal neurons	Tg(Drd1-EGFP)X60Gsat	C57B6/J
D2-GFP BAC (8) GFP in Drd2 BAC is expressed in D2-positive striatal neurons	Tg(Drd2-EGFP)S118Gsat	Mixed FVB/N and Swiss Webster
P172-mCitrine transposon (11) Piggyback enhancer trap line with tet-transactivator–driven mCitrine expressed in striosome projection neurons with age-dependence	Piggyback-Tta Line 172	C57B6/J
Sepw1-Cre NP67 BAC (10) Cre in Sepw1 BAC of Line NP67 is enriched in striosome projection neurons in the medial striatum	Sepw1-Cre NP67 BAC	Mixed C57B6/J and 129S6

Table S2. Primary antibodies

Primary antibody	Host	Company	Catalogue no.	Concentration
Connexin	Rabbit	Abcam	Ab11370	1:1,000
DAT	Rat	Millipore	MAB369	1:250
GFAP	Chicken	Abcam	Ab4674	1:1,000
GFP	Chicken	Aves Laboratory	GFP-1020	1:500
GFP (mCitrine)	Chicken	Abcam	Ab13970	1:2,000
GFP (YFP and GCaMP6)	Rabbit	Abcam	Ab6556	1:2,000
DsRed (tdTomato)	Mouse	Clontech	632393	1:250
VGluT2	Guinea Pig	Millipore	AB2251	1:5,000
GAD65/67	Rabbit	Millipore	AB1511	1:500
μ-opioid Receptor 1	Rabbit	Abcam	Ab134054	1:500

All antibodies are commercially available and have been previously validated by other researchers and companies. The basic immunoreactive patterns that we observe (at the cellular or subcellular level) are as expected, based on previous publications, for connexin, DAT, GAD65/67, GFAP, μ-opioid receptor, and VGluT2.

Table S3. Secondary antibodies

Secondary antibody	Company	Catalogue no.	Concentration
Goat anti-rabbit IgG (H+L), Alexa Fluor 633	Thermo Fisher Scientific	A-21070	1:300
Goat anti-mouse IgG (H+L), Alexa Fluor 546	Thermo Fisher Scientific	A-11030	1:300
Goat anti-chicken IgY (H+L), Alexa Fluor 488	Thermo Fisher Scientific	A-11039	1:300
Goat anti-tat IgG (H+L), Alexa Fluor 546	Thermo Fisher Scientific	A-11081	1:300
Goat anti-guinea pig IgG (H+L), Alexa Fluor 488	Thermo Fisher Scientific	A-11073	1:300
Anti-rabbit IgG (H+L), biotinylated	Vector Laboratories	BA-1000	1:500

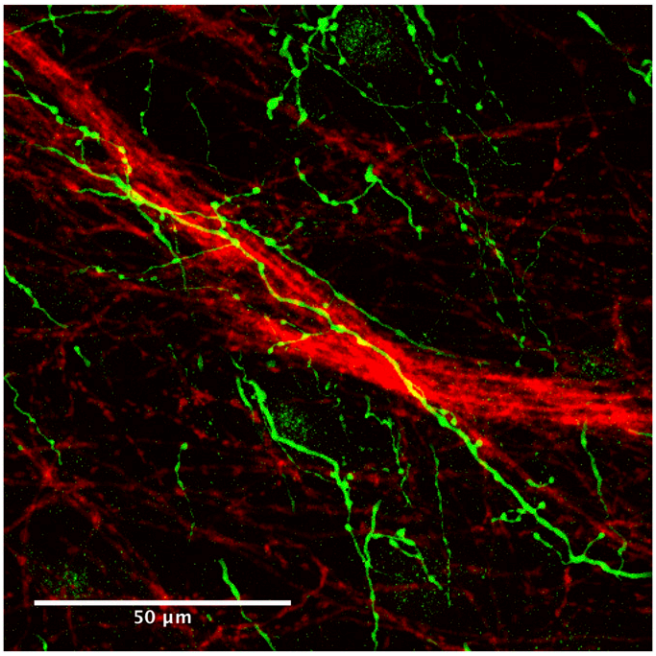

Movie S1. Animation through a Z-stack of confocal optical images, taken at 0.7-µm intervals with a standard 100× oil immersion lens, of a nigral section with cholinergic axons labeled in green and dopamine-containing fibers in red.

Movie S1